OPEN ACCESS
IOP Publishing

Made open access 12 March 2020
Journal of Physics: Condensed Matter

J. Phys.: Condens. Matter **31** (2019) 175001 (7pp)
https://doi.org/10.1088/1361-648X/ab02c5

Anisotropic 2D metallicity: plasmons in Ge(1 0 0)-Au

T Lichtenstein[1], Z Mamiyev[1,4], E Jeckelmann[2], C Tegenkamp[1,3] and H Pfnür[1,4]

[1] Institut für Festkörperphysik, Leibniz Universität Hannover, Appelstraße 2, 30167 Hannover, Germany
[2] Institut für Theoretische Physik, Leibniz Universität Hannover, Appelstraße 2, 30167 Hannover, Germany
[3] Institut für Physik, Technische Universität Chemnitz, Reichenhainer Straße 70, 09126 Chemnitz, Germany
[4] Laboratorium für Nano- und Quantenengineering (LNQE), Leibniz Universität Hannover, Schneiderberg 39, 30167 Hannover, Germany

E-mail: pfnuer@fkp.uni-hannover.de

Received 3 December 2018, revised 21 January 2019
Accepted for publication 29 January 2019
Published 27 February 2019

Abstract

The low-energy plasmonic excitations of the Ge(0 0 1)-Au close to one monolayer coverage of Au were investigated by momentum-resolved high resolution electron energy loss spectroscopy. A very weak plasmonic loss was identified dispersing along the chain direction of the $c(8 \times 2)$ formed at these Au coverages. The measured dispersion was compared with the Tomonaga–Luttinger-liquid (TLL) model and with a model for an anisotropic Fermi liquid. Using the TLL model both for single and arrays of wires, no consistent picture turned up that could describe all available data. On the contrary, a quasi-one-dimensional model of a confined 2D electron gas gave a satisfactorily consistent description of the data. From these results for the collective low-energy excitations we conclude that the Ge(0 0 1)-Au system is reasonably well described by a strongly anisotropic 2D Fermi liquid, but is incompatible with a TLL.

Keywords: low dimensional plasmons, screening, 1D versus 2D

(Some figures may appear in colour only in the online journal)

1. Introduction

Metallic systems can be reduced down to quasi-one-dimensional (1D) wires, which then exhibit a wide spectrum of new phenomena such as quantization of conductance, strong electronic correlation manifested by spin-charge separation, charge and spin density waves [1, 2], triplet superconductivity, and Luttinger liquid behavior [3–5]. Due to their inherent instability, however, structural embedding and understanding of the coupling to other dimensions is of high relevance, since it may strongly modify the properties just mentioned. Fortunately, some of the 1D properties can still be observed in these quasi-1D systems [6–10], but the investigations are not suffiently systematic yet to make clear predictions. This was one of the motivations for the present study.

The Ge(0 0 1)-Au system is one of the prototype systems for self-organized atomic chains on insulating or semiconducting surfaces [11–15] that may be able to exhibit such quasi-one-dimensional properties while being embedded in a two- or three-dimensional environment. On the other hand, it is also exemplary for the difficulties of analyzing such systems. E.g. the many structural investigations of the Au covered Ge(0 0 1) surface, mainly with diffraction [16] and tunneling microscopy [13, 17–25] did not allow to uniquely model the structure of this system. While the so-called giant missing row model was able to reproduce some of the experimental properties [26], there are quite different suggestions for the optimal Au concentration leading to the observed $c(8 \times 2)$ structure ranging from fractions of a monolayer (ML) [19–21, 24] to about one ML or even higher coverages [16, 27, 28]. Considerations of the Gibbs free energy in recent modelling [29] show that

stabilization of structures is temperature dependent with the consequence that the highly corrugated structures of the giant missing-row models [20] with concentrations above one ML are significantly more stable at and above room temperature than the dimer-row [17, 26, 30] or bridged dimer-row models [20]. While this finding may explain some of the ambiguities in the results obtained in the past, it also shows that this system is prone of formation of metastable structures that have not been explored in detail yet.

Also the electronic structure of this system was described and discussed in a very controversial manner. Photoemission and STM data were originally interpreted as being fully compatible with quasi-one-dimensional electronic properties [13, 19, 23, 31, 32] in form of a Tomonaga–Luttinger-liquid (TLL) with strong electron–electron interaction [3, 33]. However, other studies carried out with similar methods indicate [20, 24, 27, 28, 34] that this system is indeed highly anisotropic, but the Fermi surface in particular is still two-dimensional.

Since the excitation spectrum of this highly correlated system and its dynamics are still largely unexplored, which is particularly true for collectively excited states, this work utilizes electron energy loss spectroscopy (EELS) [35] in combination with low energy electron diffraction (LEED) and reports on the plasmon dispersion of the Ge(1 0 0)-Au system. As it turns out from the analysis of the data, it is difficult to reconcile the measured dispersion with one-dimensional models. Possible reasons will be discussed.

2. Experimental setup and sample preparation

The experiments were carried out in an ultra-high vacuum chamber at a base pressure below 1×10^{-10} mbar. The system hosts a high resolution spot profile analysis low energy electron diffractometer (SPA-LEED) for the investigation and control of the sample quality. The plasmon dispersion was accessed by an electron energy loss spectrometer combined with LEED to provide high resolution in both energy (10 meV) and momentum (10^{-2} Å^{-1}) [36].

The Czochralski grown Ge(1 0 0) samples were n-doped with Sb and had a specific resistance of 10 Ωcm. Since the germanium oxide layer is not a good protection against contaminants, [37] the preparation of a high-quality surface is always a demanding task, involving the ablation of several surface layers both *ex situ* by etching as well as *in situ* by several cycles of Ar^+ ion sputtering with subsequent rapid annealing at 850 °C, see e.g. [13, 38–41]. As shown in [16] in a qualitative energy-dependent analysis of the diffraction spot profiles, relating the number of sputtering/annealing cycles and the ion acceleration energy with the average terrace width and roughness, the best result was obtained for bare germanium after eight cycles with a mean terrace width of >60 nm and an RMS roughness of <1 Å. We followed the same procedures as described in [16] for the optimization of the coverage of the Au-induced reconstruction, yielding the best structural results for a coverage of 1 ML. According to theoretical modelling results [29], this structure is characterized by deep grooves,

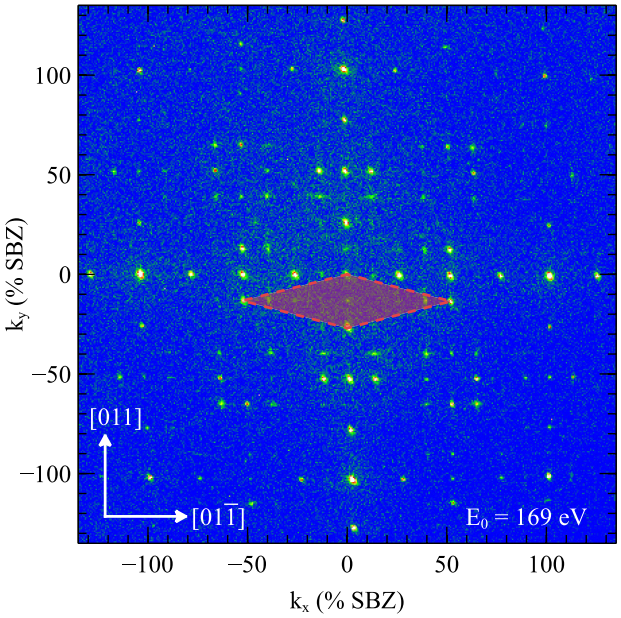

Figure 1. The LEED pattern of the Ge(1 0 0)-Au surface with a total coverage of 1.25 ML shows a $c(8 \times 2)$ reconstruction marked with a red diamond related to the Au-induced wires on the surface.

characteristic for models derived from the giant missing row model [20, 26].

Within the work presented here, we also tested the influence of the coverage on the plasmonic excitations. The appropriate amount was evaporated from a gold pearl attached to a tungsten filament by direct current heating of the filament at a deposition rate of approximately 0.15 ML min^{-1}. The sample was kept at room temperature. The coverage was controlled and calibrated with quartz microbalances placed close to the evaporator and at the position of the samples, respectively, assuming a sticking coefficient of one. After the gold adsorption, the sample was annealed at 500 °C for 10 s. Before adsorption for a new measurement, the surface was sputtered in a sequence of several cycles of Ar^+ sputtering with 800 V acceleration voltage followed by flash-annealing to 850 °C for ≈5 s. This cleaning ensured a germanium surface free of remaining gold.

3. Results and discussion

3.1. Atomic structure

The LEED pattern of the dual domain Ge(1 0 0)-Au surface right after preparation is shown in figure 1. This pattern agrees well with those of [23, 42] and is characteristic for Ge(1 0 0) with a local coverage of 1 ML of Au. Its reconstruction with a $c(8 \times 2)$ periodicity has been related to the Au-induced wires on the surface with a wire spacing of 4a (16 Å), aligned in an additional zig–zag $p(4 \times 1)$ superstructure, resulting in further spots [16, 23, 42]. The appearance of these superstructure spots are attributed to the long-range interaction between adjacent wires. Consequently, the appearance of long-range order in combination with the very sharp structural spots gives an indication of an extremely well-ordered sample. A detailed

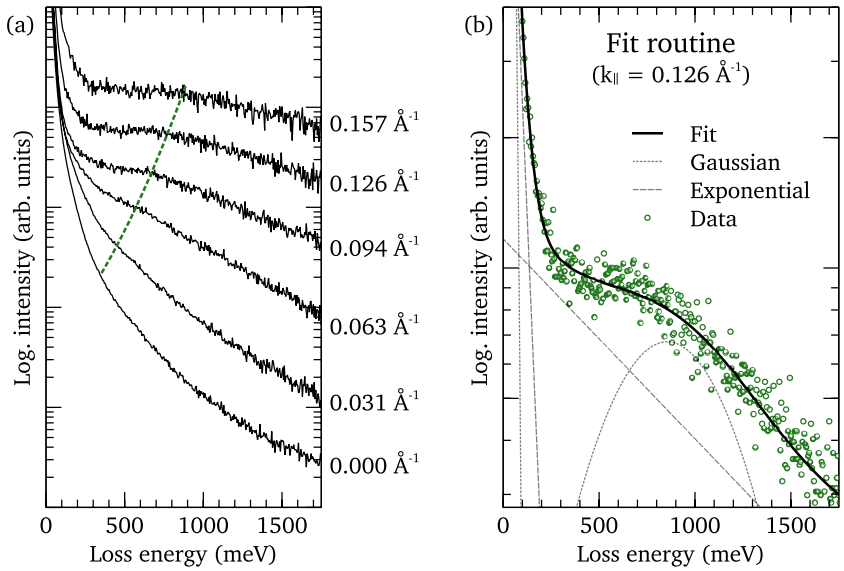

Figure 2. Electron energy loss spectra of Ge(1 0 0) with 1 ML Au coverage for various values of parallel momenta: (a) A dispersing feature can be seen for increasing momentum in the spectra given as black lines. Its shift is highlighted by the dashed line. (b) Example of the fit routine for $k = 0.126$ Å^{-1}. The data (green circles) was described by an empiric parametrization of the background, fitting the plasmon peak with a Gaussian function. The individual components are depicted by the gray dashed lines, the resulting fit by a solid black line. Please note that the scale is three orders of magnitude below the elastic intensity of the given spectrum.

investigation of the atomic structure by a energy-dependent spot profile analysis in electron diffraction showed a minimum terrace size of 200 Å that went up to more than 350 Å in presence of Au for the optimal Au coverage, confirming a high sample quality. This optimal coverage was determined to be 1 ML. Any excess coverage exceeding 1 ML results in growth of small Au-clusters on the surface [25] that are not visible in LEED, and do not lead to low-energy plasmons (see below). The chains of the $c(8 \times 2)$ reconstruction are several atoms high, as indirectly concluded from an RMS roughness of $\approx$ 3 Å and an increase in double, triple and sextuple height correlations [16, 43], supporting a structure with deep trenches.

3.2. Plasmonic excitations in the loss spectra

On these well-ordered surfaces, angle resolved electron energy loss spectroscopy measurements were performed. Figure 2(a) shows an exemplary sequence of these spectra on a semi-log scale as a function of increasing $k_{\|}$ for a sample with 1 ML Au coverage. Here, $k_{\|}$ denotes a measurement in $[0\,1\,\bar{1}]$ direction. No difference was seen when measuring in $[0\,1\,1]$ direction. This behavior is expected, since the surface exhibits two domains rotated by 90° that exist with equal probability on the surface. All data were normalized to the intensity of the elastic peaks of each spectrum and shifted upward in intensity with increasing k for better visibility. The accumulated integration time of the plotted curves was $\approx$10 s per data point with a step width of 5 meV. These time-consuming settings were necessary due to the very low intensity of the plasmonic signal, as also directly visible from the spectra.

Figure 2(b) shows a magnified view of the loss spectrum for $k_{\|} = 0.126$ Å^{-1}. On top of the data marked by circles, the obtained fit is plotted. This fit is the sum of the following parametrization: Gaussian-type functions describe the elastically scattered as well as the loss peak, exponential functions approximate the Drude background. This so-called Drude-tail is an indicator for the metallic character and has its roots in the continuum of excitation of electron–hole pairs in a metal [44, 45]. It is also seen in other low-dimensional systems [46, 47].

Compared to basically all low-dimensional plasmons investigated in the last decades [48–53], the loss peak associated with a plasmon excitation has extremely low intensity and shows a very broad full width at half maximum (FWHM). These properties also result in a high uncertainty of the exact position of the plasmon peak during the fitting process, as reflected by the high scatter of the extracted data in figure 3. Furthermore, the decay of the intensity next to the elastic peak is very flat, indicating a low probability of single particle excitations. In spite of the low excitation probability, a dispersing feature that shifts to higher energies with increasing k is visible in the spectra of figure 2(a), highlighted by the dashed curve.

Measurements were also carried out for Au coverages from 0.5 ML to 2 ML. The accuracy of the coverage was around 10%. No differences to the curves shown in figure 2 as a function of the amount of Au were found. This insensitivity to the Au concentration is in agreement with the finding that upon adsorption the gold-covered superstructure grows in patches [18] with the subsequent formation of excess gold clusters above 1 ML that cannot contribute to the low-energy plasmon [25]. In conclusion, the plasmon occurs in locally reconstructed parts that form Au for coverages >0.5 ML.

3.3. Dispersion of the plasmonic excitation

All obtained spectra were analyzed as described above and according to the procedure depicted in figure 2(b). The dispersion of these extracted data together with two possible descriptive models are plotted in figure 3.

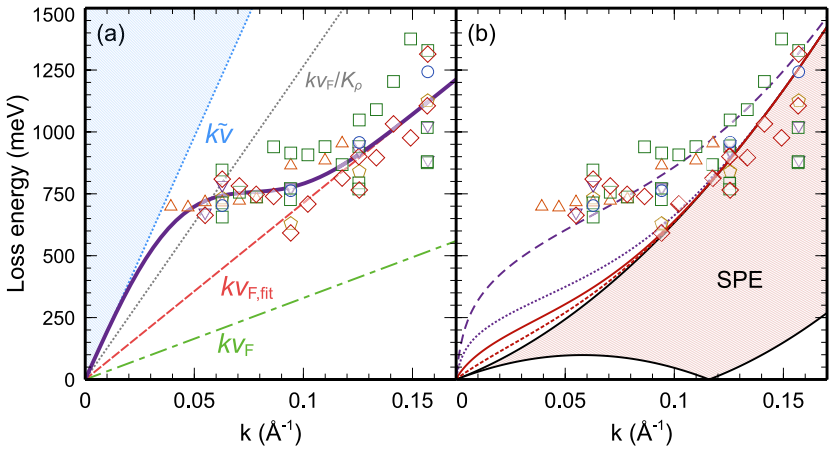

Figure 3. Plasmon dispersion extracted from loss measurements and comparison with two models for the plasmon dispersion relation. No dependence on Au coverage was found, as indicated by the different symbols (◯: 0.5 ML, ◇: 0.75 ML, □: 1.0 ML, △: 1.2 ML, ▽: 1.5 ML, ⬠: 2.0 ML). (a) Comparison with the one-dimensional TLL model in combination with a screened electron- electron interaction described by a Gaussian distribution. The resulting fit is given by the purple line. $kv_{F,fit}$ from this fit (red dashed line) is not close to kv_F derived from photoemission (green dash-dotted line). Grey dotted line: kv_F/K_ρ with $K_\rho = 0.26$, as derived from [31]. $k\tilde{v}$ obtained as limiting slope of the thick dark curve. Further details, see text. (b) Comparison with the plasmon dispersion derived from a confined quasi-free 2D electron gas model. Plasmon dispersion of a single wire (dashed red) and an array of wires (solid red), both with a width of $w = 5$ Å, as well as for an array of wires with $w = 20$ Å (dotted purple). The long dashes mark the 2D plasmon dispersion using the same parameters for electron density and effective mass. The shaded area shows the electron–hole excitation continuum (SPE).

Unfortunately, due to their small intensities, the centers of the Gaussian part of the plasmon could only be determined for k values above 0.04 Å^{-1}. For $k < 0.1$ Å^{-1} the data level off at around 700 meV, whereas for shorter wavelengths (higher k) the plasmon loss energy increases steadily as a function of k. A first attempt to explain the almost constant loss energy at small k is to assume a finite wire length that leads to standing waves and, consequently, to no dispersion for low k. However, the structural investigations of [16] reveal minimum terrace sizes of 200 Å. If this terrace size also limits the length of wires, this origin does not seem to be very likely: if we assume that the quasi-linear dispersion seen at large $k_\parallel$ extends to zero energy for the ideal system, but is cut off by finite size effects at the measured plateau at 700 meV, the intersection where free dispersion starts is approximately at $k_\parallel = 0.1$ Å. From this value an effective wire length of merely 30 Å is derived. Therefore, only if the wires are highly defective, finite size effects would yield an acceptable explanation for our findings.

In view of recent results from photoemission and STM [34], where it was shown that this system is strongly anisotropic, but not one-dimensional, we test in the following two extremes of one-dimensional electron models and basically demonstrate inconsistency with a 1D description also for the plasmon excitations. These approaches are a modified Tomonaga–Luttinger-liquid model and a quasi-free 1D electron gas with a finite lateral extent.

3.4. Description by a modified Tomonaga–Luttinger-liquid model

In the strictly one-dimensional TLL model with the assumption of a linear single-electron excitation spectrum close to the Fermi energy [4], the plasmon dispersion is also linear in k for $k \to 0$,

$$\omega_p(k) = k u_\rho(k) = k v_F \underbrace{\sqrt{1 + \frac{2v_c(k)}{\hbar\pi v_F}}}_{1/K_\rho(k)} \tag{1}$$

but with a k-dependent velocity of propagation $u_\rho(k)$ that can be described as the Fermi velocity, v_F, renormalized by the Luttinger parameter $K_\rho(k)$ for charge excitations. This parameter depends on the Fourier transform of the screened electron–electron interaction, $v_c(k)$.

An isotropically screened Coulomb potential is generally used as restoring potential for the plasmon [4, 54]. Contrary to the observation, however, such a potential leads to a dispersion relation that cannot reproduce the non-monotonic curvature seen in our experimental data. Hence, this model had to be extended by an effective electron–electron potential in the wire that is assumed to be cut off beyond some wave number k_{crit}, as also already introduced in context with a TLL elsewhere [55]. Its Fourier-transformed representation in the wire direction is expressed by

$$v_c(k) = \alpha\pi\hbar v_F \exp\left(-k^2/k_{crit}^2\right) \tag{2}$$

which then defines the resulting dispersion to first order in the potential strength as

$$\omega_p(k) = v_F k \left(1 + \alpha \exp\left(-k^2/k_{crit}^2\right)\right). \tag{3}$$

A reasonable fit of the data (see figure 3) was obtained setting $v_F = 1.08 \times 10^6$ m s^{-1}, $\alpha = 2.0$, and $k_{crit} = 0.06$ Å^{-1}. This means that electronic screening is of extremely long range (40 Å), corresponding to a screening length that is much larger than the interchain distance d. Thus coupling between wires seems to be inevitable so that this finding already casts doubt on the applicability of this model.

Although the resulting parameters perfectly describe the data, there are further problems with this model. First of all, for high k the dispersion aligns to a $v_{\mathrm{F,fit}}$ that is twice as large as the Fermi velocity v_{F} obtained from photoemission [56] and from tight-binding calculations [34]. The fit result is indicated by the red dashed line, the resulting dispersion with v_{F} from photoemission [34, 56] as green dash-dotted line in figure 3(a). Furthermore, if the evaluation of STS data [31] with the TLL theory is taken as correct, it yields $K_\rho = K_\rho(k \to 0) = 0.26$. This value, however, should renormalize the velocity to $u = v_{\mathrm{F}}/K_\rho \approx 4v_{\mathrm{F}}$ for $k = 0$, shown by the grey dotted line. It is not consistent with the extrapolation to zero and its initial slope, as marked by the blue dotted line. Due to the lack of data points for low k, we can only derive a lower bound $\tilde{v} = (1+\alpha)v_{\mathrm{F,fit}} \approx 6v_{\mathrm{F}}$ for the velocity u in that limit. This would imply $K_\rho \lesssim 0.17$ which is significantly smaller than the prediction from STS mentioned above. The region filled in bright blue is the corresponding region for these values.

It is quite difficult to determine the properties of coupled TLL wires [4, 57, 58]. However, the two-dimensional plasmon dispersion $\omega_{\mathrm{p}}(\vec{k})$ can be calculated if we assume that the TLL chains are only coupled by an isotropically screened electron–electron interaction [59]. Applying the results of [59] to a two-dimensional array of TLL wires, we obtain a dispersion

$$\omega_{\mathrm{p}}(\vec{k}) = k_x u_\rho(|\vec{k}|) \tag{4}$$

where k_x is the wave number in the wire direction and the renormalized velocity $u_\rho(|\vec{k}|)$ is given by an expression similar to equation (1) but with the two-dimensional Fourier transform of the screened electron–electron potential. Assuming a two-dimensional version of the effective Gaussian potential (2) and the Luttinger parameter $1/K_\rho = \sqrt{1+2\alpha}$ obtained from STS, the experimental plasmon dispersions can now be reproduced with an isotropic screening length equal to twice the interchain distance d and a strong-coupling potential $\alpha \approx 7$. The resulting dispersion $\omega_{\mathrm{p}}(\vec{k})$ depends significantly on the wave number k_y perpendicular to the wires, however, and thus characterizes more a strongly anisotropic and correlated two-dimensional metallic state than weakly coupled TLL wires. Moreover, the fitted Fermi velocity $v_{\mathrm{F,fit}}$ remains incompatible with the Fermi velocity v_{F} obtained from photoemission.

In summary, these contradicting results are not compatible with the TLL theory of a correlated quasi-1D electron system and rule out the presence of a such a behavior, in agreement with [34, 60]. Both STM and the latest photoemission data [60, 61] suggest the electronic system to be highly anisotropic with the formation of wire-like structures, which in the limit of strong confinement is equivalent to a coupled array of wires. Therefore, we now tested, as described in the next section, a quasi-one-dimensional quasi-free electron gas model with coupling between wires.

3.5. Description by a quasi-free electron gas model with 1D confinement

This approach has been successfully applied to systems like Si(557)-Au [62]. The plasmon dispersion of a quasi-free 1D electron gas can generally be expressed by [63]

$$\omega_{\mathrm{p}}(k) = \sqrt{\frac{\omega_+^2\, \mathrm{e}^{A(k)} - \omega_-^2}{\mathrm{e}^{A(k)} - 1}} \tag{5}$$

with $\omega_\pm$ as the upper and lower boundary of the single electron–hole pair continuum. $A(k)$ is a function describing the electronic correlations of the system. Both are defined as:

$$\omega_\pm = \frac{\hbar(k^2/2 \pm k k_{\mathrm{F}})}{m^*}, \quad A(k) = \frac{\hbar^2 2\pi k}{m^* g_s v_c(k)} \times \frac{1}{1 - G_{\mathrm{corr}}(k)}. \tag{6}$$

Here, k_{F} is the Fermi wave vector, m^* is the effective mass of the electrons, and g_s is the spin degeneracy factor that can be either 2 or 1. The Coulomb interaction is again treated by its Fourier transformed representation $v_c(k)$. In contrast to the TLL model, all electrons contribute to $v_c(k)$, i.e. also those electrons of the conducting channel. Additionally, for the calculations of this work, the local field correction factor $G_{\mathrm{corr}}(k)$ originates in a self consistent mean-field approximation developed by Singwi, Tosi, Land and Sjlander [64] to consider electronic correlations it is often abbreviated as STLS.

For a description for our plasmon, the electronic structure of the Ge(1 0 0)-Au system was fit with a parabola to $m^* = 0.13 m_{\mathrm{e}}$ and $k_{\mathrm{F}} = 0.058$ Å^{-1} in direction parallel to the wires [31, 34].

The Coulomb interaction $v_c(k)$ was calculated numerically. It is expressed, in analogy to [63, 65, 66], by

$$v_c(k) = \frac{e^2}{2\bar{\epsilon}\epsilon_0} \int \mathrm{d}y \int \mathrm{d}\tilde{y}\, |\phi(y)|^2 |\phi(\tilde{y})|^2 \times K_0\left(k|y-\tilde{y}|\right). \tag{7}$$

In this expression, e is the elementary charge, $\bar{\epsilon}\epsilon_0$ the average permittivity of the surrounding media, and K_0 is the zeroth order modified Bessel function of second kind. In this work, the absolute square of the electron wave function perpendicular to the channel $|\phi(\tilde{y})|^2$, i.e. the lateral extension of a wire, was approximated by a Gaussian. In other word the confining potential was assumed to be harmonic.

As the wires arrange themselves into arrays, there is an infinite number of additional electronic channels in the vicinity of an isolated wire with interwire spacing d. In a simple approach, this will add a term to the Coulomb matrix element describing the influence of the additional electron density [67]:

$$v_c^{\mathrm{eff}}(k) = \underbrace{v_c(k)}_{\text{intrawire}} + \underbrace{v_c^{\mathrm{array}}(k)}_{\text{interwire}}. \tag{8}$$

This additional Coulomb interaction can be described by the following integral [65]:

$$v_c(k)^{\mathrm{array}} = \frac{e^2}{\bar{\epsilon}\epsilon_0} \int \mathrm{d}y \int \mathrm{d}\tilde{y}\, |\phi(y)|^2 |\phi^{\mathrm{array}}(\tilde{y})|^2 \times K_0\left(k|y-\tilde{y}|\right). \tag{9}$$

In the present case, the system was modeled with FWHM = 5 Å of $|\phi(y)|^2$ and an interchain distance of $d =$ 16 Å, see figure 4(a) for the lateral distribution. This choice of the wire width seems to be reasonable by comparison with STM data [19, 25]. The integral was calculated with five wires to both sides of the conduction channel. Wires further away have a negligible influence on the value of $v_c(k)$. The relative

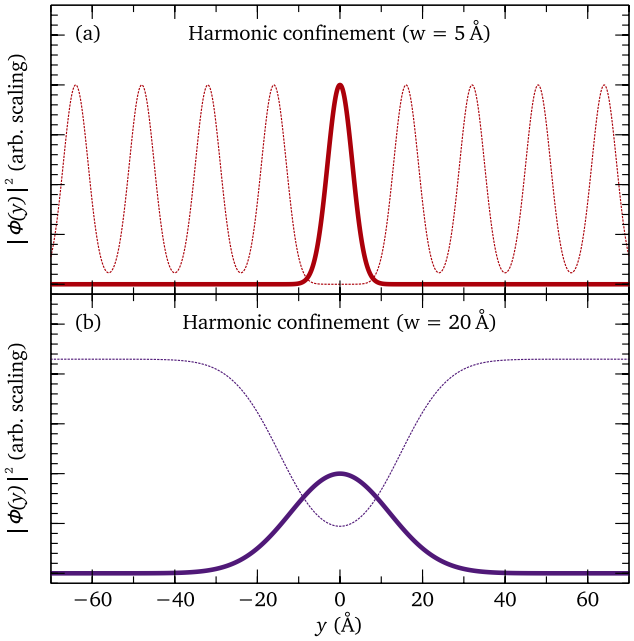

Figure 4. Absolute squares of the wave functions of varying widths for the description of the Ge(1 0 0)-Au plasmon. Changing the width from 5 Å (a) to 20 Å (b) leads to a strong overlap in the surrounding probability density.

dielectric constant was chosen as the mean value of germanium and vacuum as $\bar{\epsilon} = (16.2 + 1)/2 = 8.6$.

The resulting plasmonic dispersion is plotted in figure 3(b) by the dashed red line for a single wire and by the solid red line for a wire placed within an array of wires. For large $k > 0.09$ Å^{-1}, there is a good agreement between the data and the calculation. This conformity is mainly attributed to the behavior of the upper boundary of the electron–hole single-particle excitation spectrum (SPE). For lower k-values, however, the calculated plasmon dispersion is clearly below the experimental data both for the coupled array as well as for the single wire. Since an increasing overlap of the wave functions also increases the plasmonic energy at long wavelengths, the same calculation was carried out for an effective width of the wave function of $w = 20$ Å of each wire, which results in a very large overlap of wave functions of adjacent wires. To include this overlap appropriately, the numerics were carried out in an array of 51 such wires. In total, the system now corresponds to a wider channel in an effective 2D environment. The resulting dispersion relation shows a trend towards the experimental data, which is depicted by the dotted purple curve in figure 3. However, it is still not possible to get the calculated curve close to the experimental data for $k < 0.1$ Å.

A possible explanation is the elliptic two-dimensional Fermi surface [34]. The strongly anisotropic electronic band structure yields a much higher effective mass perpendicular to the wires compared to the parallel direction. These strongly anisotropic 2D properties are obviously not correctly described by our 1D or quasi-1D models. While the difference in electronic structure also leads to anisotropic conduction properties, an additional perpendicular conduction channel leads to a substantial delocalization of electronic states. This crossover to two dimensions, although modeled by the stretch-out of the wave functions in the given case, might need a better description.

Since our samples were dual-domain samples, there is no information about the direction perpendicular to the actual direction of measurement. Therefore, there is a third possibility, namely again the case of strong confinement. In that case, there is the possibility that we observe as dominant loss at low k the first subband excitation at $k_y = 0$ in the confining potential perpendicular to the wires when the dispersion measurement is along the x-direction. Indeed, if we assume a square well potential for a single wire with an effective mass of the electrons of $0.13\,m_e$ [34], we obtain an effective wire width of about 15 Å from the measured excitation energy of about 700 meV. This width is close to the actual wire width. Since the short wavelength (high k) data agree with model calculations, compatibility with the quasi-1D model may be concluded. However, this range of data is not very specific to a concrete model. Angle-dependent measurements on single-domain samples should help to shed more light on this issue. Such an approach is possible on Ge(1 0 0) wafers with an intentional miscut in [0 1 1] direction. However, those samples did not show any plasmonic excitation. This effect is most likely caused by a very strong damping, typical for stepped samples [68].

4. Conclusions

Our results of plasmon dispersion in Au wires on Ge(0 0 1) show that 1D plasmon models are not compatible with experimental data, if the effective masses and electron densities known from angular resolved photoemission are used. These results are in agreement with latest results from STM and ARPES [34, 60, 61] which suggest the Ge(1 0 0)-Au system to be a strongly anisotropic 2D metal, but with highest dispersion of bands close to E_F not parallel, but perpendicular to the wire direction. While this finding is compatible with our data, there are, however, still many open questions, which are only partly due to a still incomplete set of data. Our work shows that a high quality of long range order does not guarantee the perfect formation of plasmonic waves. At this moment we can only speculate why in this system damping is much more efficient than in the comparable Si(hhk)-Au systems.

Acknowledgments

This work was supported by the Deutsche Forschungsgemeinschaft within Research Unit 1700, projects E4 and T2.

ORCID iDs

C Tegenkamp https://orcid.org/0000-0003-0453-0765
H Pfnür https://orcid.org/0000-0003-1568-4209

References

[1] Grüner G 1988 *Rev. Mod. Phys.* **60** 1129
[2] Kagoshima S, Nagasawa H and Sambongi T 1988 *One-Dimensional Conductors* (*Springer Series in Solid-State Sciences* vol 72) (Berlin: Springer) pp 126–135
[3] Luttinger J M 1963 *J. Math. Phys.* **4** 1154
[4] Giamarchi T 2003 *Quantum Physics in One Dimension* (Oxford: Clarendon)
[5] Schönhammer K 2004 Luttinger liquids: basic concepts *Strong Interactions in Low Dimensions* (*Physics and Chemistry of Materials with Low-Dimensional Structures* vol 25) ed L D D Baeriswyl (Dordrecht: Springer) ch 4 pp 93–136
[6] Zeng C, Kent P, Kim T-H, Li A-P and Weitering H H 2008 *Nat. Mater.* **7** 539
[7] Snijders P C and Weitering H H 2010 *Rev. Mod. Phys.* **82** 307
[8] Weitering H 2011 *Nat. Phys.* **7** 744
[9] Aulbach J, Schäfer J, Erwin S C, Meyer S, Loho C, Settelein J and Claessen R 2013 *Phys. Rev. Lett.* **111** 137203
[10] Brand C, Pfnür H, Landolt G, Muff S, Dil J H, Das T and Tegenkamp C 2015 *Nat. Commun.* **6** 8118
[11] González C, Flores F and Ortega J 2006 *Phys. Rev. Lett.* **96** 136101
[12] Erwin S C and Himpsel F J 2010 *Nat. Commun.* **1** 58
[13] Blumenstein C, Meyer S, Ruff A, Schmid B, Schäfer J and Claessen R 2011 *J. Chem. Phys.* **135** 064201
[14] Cheon S, Kim T-H, Lee S-H and Yeom H W 2015 *Science* **350** 182
[15] Frigge T *et al* 2017 *Nature* **544** 207
[16] Lichtenstein T, Teiken H, Pfnür H, Wollschläger J and Tegenkamp C 2015 *Surf. Sci.* **632** 64
[17] Wang J, Li M and Altman E I 2004 *Phys. Rev.* B **70** 233312
[18] Wang J, Li M and Altman E 2005 *Surf. Sci.* **596** 126
[19] Schäfer J, Blumenstein C, Meyer S, Wisniewski M and Claessen R 2008 *Phys. Rev. Lett.* **101** 236802
[20] van Houselt A, Fischer M, Poelsema B and Zandvliet H J W 2008 *Phys. Rev.* B **78** 233410
[21] Gallagher M C, Melnik S and Mahler D 2011 *Phys. Rev.* B **83** 033302
[22] Niikura R, Nakatsuji K and Komori F 2011 *Phys. Rev.* B **83** 035311
[23] Blumenstein C, Meyer S, Mietke S, Schäfer J, Bostwick A, Rotenberg E, Matzdorf R and Claessen R 2013 *J. Phys.: Condens. Matter* **25** 014015
[24] Park J, Nakatsuji K, Kim T-H, Song S K, Komori F and Yeom H W 2014 *Phys. Rev.* B **90** 165410
[25] Safaei A, van Houselt A, Poelsema B, Zandvliet H J W and van Gastel R 2013 *Phys. Rev.* B **88** 085415
[26] Sauer S, Fuchs F, Bechstedt F, Blumenstein C and Schäfer J 2010 *Phys. Rev.* B **81** 075412
[27] Nakatsuji K, Motomura Y, Niikura R and Komori F 2011 *Phys. Rev.* B **84** 115411
[28] Nakatsuji K and Komori F 2012 *Nat. Phys.* **8** 174
[29] Seino K, Sanna S and Schmidt W G 2018 *Surf. Sci.* **667** 101
[30] Tsay S-F 2016 *J. Phys.: Condens. Matter* **28** 435001
[31] Blumenstein C, Schäfer J, Mietke S, Meyer S, Dollinger A, Lochner M, Cui X Y, Patthey L, Matzdorf R and Claessen R 2011 *Nat. Phys.* **7** 776
[32] Meyer S, Dudy L, Schäfer J, Blumenstein C, Höpfner P, Umbach T E, Dollinger A, Cui X Y, Patthey L and Claessen R 2014 *Phys. Rev.* B **90** 125409
[33] Tomonaga S I 1950 *Prog. Theor. Phys.* **5** 544
[34] de Jong N, Heimbuch R, Eliëns S, Smit S, Frantzeskakis E, Caux J-S, Zandvliet H J W and Golden M S 2016 *Phys. Rev.* B **93** 235444
[35] Rocca M 1995 *Surf. Sci. Rep.* **22** 1
[36] Claus H, Büssenschütt A and Henzler M 1992 *Rev. Sci. Instrum.* **63** 2195
[37] Loscutoff P W and Bent S F 2006 *Annu. Rev. Phys. Chem.* **57** 467
[38] Zhang X-J 1993 *J. Vac. Sci. Technol.* A **11** 2553
[39] Phabhakaran K, Maeda F, Watanabe Y and Ogino T 2000 *Appl. Phys. Lett.* **76** 2244
[40] Kiantaj K, Osborn T K and Kummel A C 2012 *2012 Int. Silicon–Germanium Technol. Device Meet.* (IEEE) pp 1–2
[41] Räthel J, Speiser E, Esser N, Bass U, Meyer S, Schäfer J and Geurts J 2012 *Phys. Rev.* B **86** 035312
[42] Mocking T F, Stam D, Poelsema B and Zandvliet H J W 2010 *Surf. Sci.* **604** 2021
[43] Lichtenstein T 2017 Plasmons in gold-induced quantum wires *PhD Thesis* Leibniz Universität Hannover
[44] Backes U and Ibach H 1981 *Solid State Commun.* **40** 575
[45] Persson B and Demuth J 1984 *Phys. Rev.* B **30** 5968
[46] Rugeramigabo E P, Nagao T and Pfnür H 2008 *Phys. Rev.* B **78** 155402
[47] Krieg U, Brand C, Tegenkamp C and Pfnür H 2013 *J. Phys.: Condens. Matter* **25** 014013
[48] Nagao T *et al* 2010 *Sci. Technol. Adv. Mater.* **11** 054506
[49] Politano A and Chiarello G 2015 *Prog. Surf. Sci.* **90** 144
[50] Pfnür H, Tegenkamp C and Vattuone L 2019 *Springer Handbook of Surface Science* (Heidelberg: Springer) in preparation (arXiv:1701.05049)
[51] Lichtenstein T, Mamiyev Z, Sanna S, Schmidt W G, Tegenkamp C and Pfnür H 2018 *Phys. Rev.* B **97** 165421
[52] Sanna S, Lichtenstein T, Mamiyev Z, Tegenkamp C and Pfnür H 2018 *J. Phys. Chem.* C **122** 25580
[53] Mamiyev Z, Lichtenstein T, Tegenkamp C, Braun C, Schmidt W G, Sanna S and Pfnür H 2018 *Phys. Rev. Mater.* **2** 066002
[54] Gold A and Ghazali A 1990 *Phys. Rev.* B **41** 8318
[55] Heyl M, Kehrein S, Marquardt F and Neuenhahn C 2010 *Phys. Rev.* B **82** 033409
[56] Meyer S, Schäfer J, Blumenstein C, Höpfner P, Bostwick A, McChesney J L, Rotenberg E and Claessen R 2011 *Phys. Rev.* B **83** 121411
[57] Kopietz P, Meden V and Schönhammer K 1995 *Phys. Rev. Lett.* **74** 2997
[58] Kopietz P, Meden V and Schönhammer K 1997 *Phys. Rev.* B **56** 7232
[59] Schulz H J 1983 *J. Phys. C: Solid State Phys.* **16** 6769
[60] Yaji K *et al* 2018 *J. Phys.: Condens. Matter* **30** 075001
[61] Dudy L, Aulbach J, Wagner T, Schäfer J and Claessen R 2017 *J. Phys.: Condens. Matter* **29** 433001
[62] Nagao T, Yaginuma S, Inaoka T and Sakurai T 2006 *Phys. Rev. Lett.* **97** 116802
[63] Moudgil R K, Garg V and Pathak K N 2010 *J. Phys.: Condens. Matter* **22** 135003
[64] Singwi K S, Tosi M P, Land R H and Sjölander A 1968 *Phys. Rev.* **176** 589
[65] Das Sarma S and Lai W Y 1985 *Phys. Rev.* B **32** 1401
[66] Das Sarma S and Hwang E 1996 *Phys. Rev.* B **54** 1936
[67] Inaoka T and Nagao T 2007 *Mater. Trans.* **48** 718
[68] Langer T, Baringhaus J, Pfnür H, Schumacher H W and Tegenkamp C 2010 *New J. Phys.* **12** 1